NSTX-U

Supported by U.S. DEPARTMENT OF ENERGY | Office of Science

Benchmarking

J.W. Berkery

Department of Applied Physics, Columbia University, New York, NY, USA

Rochester, New York
March 15, 2012

Coll of Wm & Mary
Columbia U
CompX
General Atomics
FIU
INL
Johns Hopkins U
LANL
LLNL
Lodestar
MIT
Lehigh U
Nova Photonics
Old Dominion
ORNL
PPPL
Princeton U
Purdue U
SNL
Think Tank, Inc.
UC Davis
UC Irvine
UCLA
UCSD
U Colorado
U Illinois
U Maryland
U Rochester
U Tennessee
U Tulsa
U Washington
U Wisconsin
X Science LLC

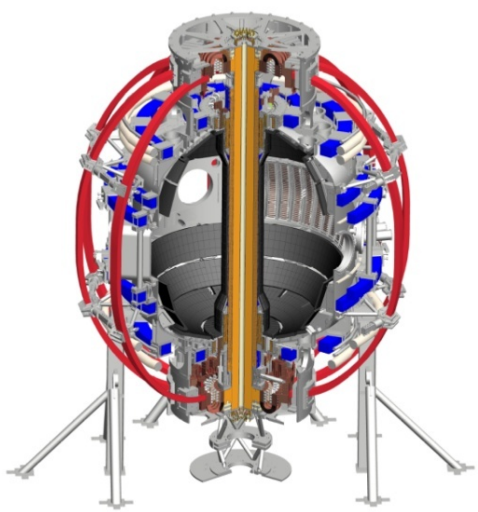

Culham Sci Ctr
York U
Chubu U
Fukui U
Hiroshima U
Hyogo U
Kyoto U
Kyushu U
Kyushu Tokai U
NIFS
Niigata U
U Tokyo
JAEA
Inst for Nucl Res, Kiev
Ioffe Inst
TRINITI
Chonbuk Natl U
NFRI
KAIST
POSTECH
Seoul Natl U
ASIPP
CIEMAT
FOM Inst DIFFER
ENEA, Frascati
CEA, Cadarache
IPP, Jülich
IPP, Garching
ASCR, Czech Rep

MDC-2 Benchmarking of kinetic models: overview & steps

- Codes: HAGIS, MARS-K, MISK
- Choice of equilibria for benchmarking

Spring 2011

  – Start by using Solov'ev
    - HAGIS / MARS-K, and MISK / MARS-K benchmarked to different degrees using Solov'ev equilibria; collect/cross compare results
      – HAGIS/MARS results published [Y. Liu et al., Phys. Plasmas **15**, 112503 (2008)]
    - Simplicity may lead to unrealistic anomalies – better to use realistic cases?
  – Move on to ITER-relevant equilibria
    - Use Scenario IV, or new equilibria recently generated for WG7 task by Y. Liu (more realistic; directly applicable to ITER)
  – Need kinetic profiles as well as fluid pressure
- Approach to stability comparison – start with
  – ideal fluid quantities ($\delta W^{no\text{-}wall}$, δW^{wall}, etc.)
  – n = 1 (consider n > 1 in a future step)
  – perturbative approach on static eigenfunction input - ensure that unstable eigenfunction is consistent among codes (e.g. no-wall ideal for MISHKA)
  – no-wall / with-wall β_N limits (equilibrium β scan needed)

Fall 2011

Initial comparison of stability calculations for Solov'ev, ITER cases (Oct. 2011)

Work in progress!

	r_{wall}/a	Ideal δW $/(-\delta W_\infty)$	$Re(\delta W_K)$ $/(-\delta W_\infty)$	$Im(\delta W_K)$ $/(-\delta W_\infty)$	$\gamma\tau_w$	$\omega\tau_w$	δW_K $/(-\delta W_\infty)$ $(\omega_E \rightarrow \infty)$
Solov'ev 1	1.15						
(MARS-K)		1.187	0.0256	-0.0121	0.804	-0.0180	0.157
(MISK)		1.122	0.0243	0.0280	0.850	-0.0452	0.236
Solov'ev 3	1.10						
(MARS-K)		1.830	0.208	-0.343	0.350	-0.228	
(MISK)		2.337	0.371	0.060	0.232	-0.027	0.689
ITER	1.50						
(MARS-K)		0.682	141.5	2.286	-0.988	0.00019	
(MISK)		0.677	0.665	-0.548	0.071	0.437	8.46

- Calculations from MISK, and MARS-K (perturbative)
  - Good agreement on ideal δW, Solov'ev 1 $Re(\delta W_K)$, $\gamma\tau_w$
  - Less agreement on Solov'ev 3, $\omega\tau_w$
  - Very different ITER result (do we have different input?)

We have compared results for Solov'ev 1 case broken down into particle types, and they do not agree.

MISK now has the ability to separate l=0 and l≠0 components.

$\delta W_K / -\delta W_\infty$ for MISK (blue) and MARS-K (red)

	thermal ions						thermal electrons		Alfvén Layer		Total	
	trapped				circulating		trapped ($l = 0$ only)					
	$l = 0$		$l \neq 0$									
	real	imag	real	imag	real	imag	real	imag	real	imag	real	imag
Solov'ev 1	8.46×10^{-2} 1.45×10^{-2}	-1.48×10^{-2} 2.23×10^{-6}	3.10×10^{-3} 3.84×10^{-3}	-5.11×10^{-5} 8.12×10^{-3}	-2.10×10^{-3} -8.90×10^{-3}	-1.33×10^{-4} 2.05×10^{-2}	-6.00×10^{-2} 1.58×10^{-2}	2.95×10^{-3} 3.68×10^{-5}	0	0	2.56×10^{-2} 2.51×10^{-2}	-1.21×10^{-2} 2.87×10^{-2}
Solov'ev 3	1.90×10^{-1}	2.50×10^{-6}	-8.69×10^{-3}	1.45×10^{-2}	4.03×10^{-3}	3.93×10^{-2}	1.90×10^{-1}	6.46×10^{-5}	-3.81×10^{-5}	-1.20×10^{-5}	2.08×10^{-1} 3.71×10^{-1}	-3.43×10^{-1} 1.46×10^{-2}
ITER	8.52×10^{-1}	3.05×10^{-4}	-9.96×10^{-2}	2.68×10^{-2}	-2.23×10^{-1}	3.78×10^{-2}	1.35×10^{-1}	-1.64×10^{-2}	-1.03×10^{-2}	-7.95×10^{-1}	6.53×10^{-1}	-7.46×10^{-1}

MISK frequency calculation improved by analytic calculation of integrals involving $1/v_{||}$ at $v_{||} \rightarrow 0$. Note: does not affect the outcome very much.

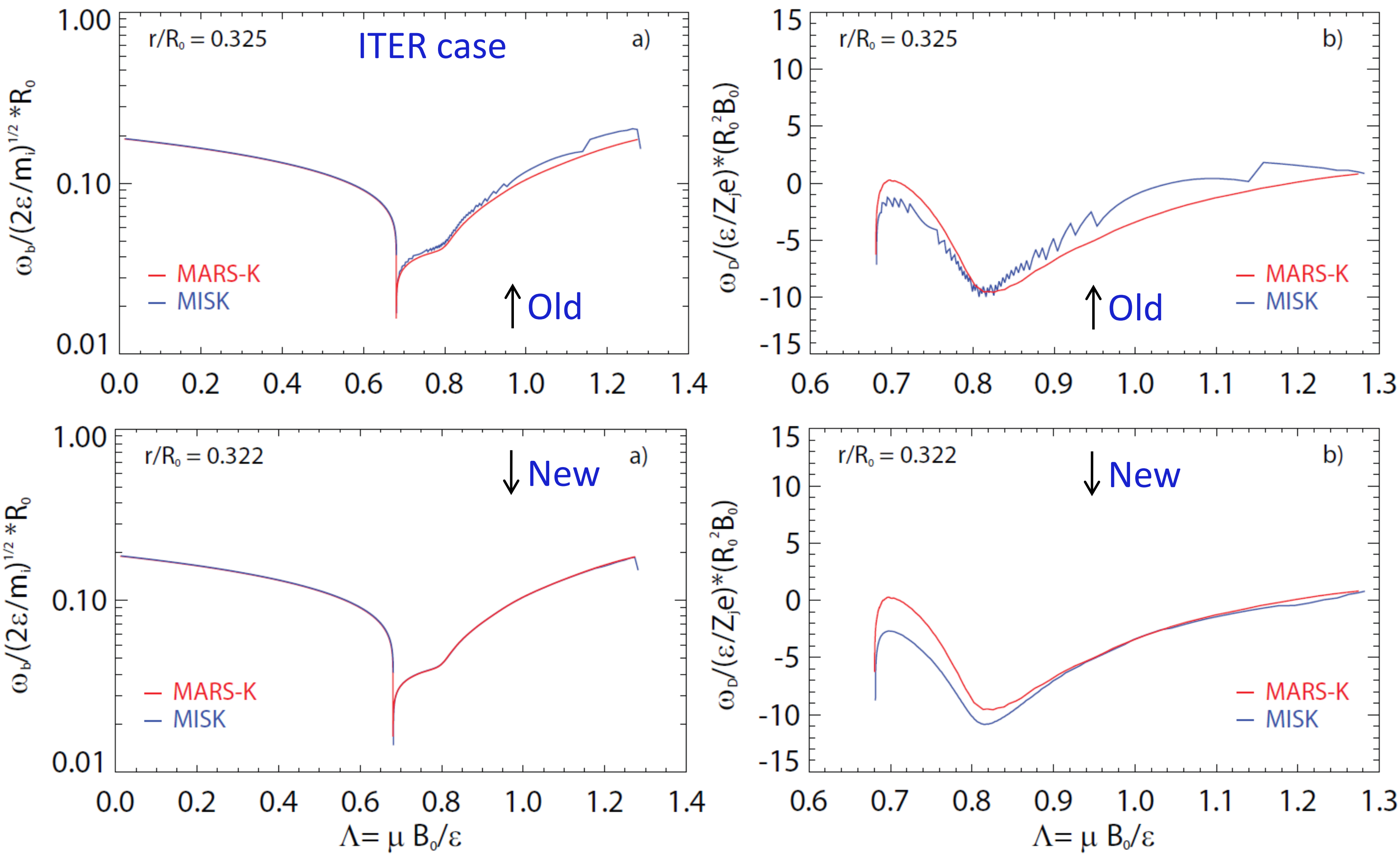

MISK calculates the energy integral numerically, MARS-K does it analytically

$$I_\varepsilon(\Psi,\Lambda,l) = \int_0^\infty \frac{n\left(\omega_{*N} + \left(\hat{\varepsilon} - \frac{3}{2}\right)\omega_{*T}\right) + n\omega_E - \omega_r - i\gamma}{n\left(\omega_D + (l + \alpha n q)\,\omega_b\right) - i\nu_{\text{eff}} + n\omega_E - \omega_r - i\gamma}\hat{\varepsilon}^{\frac{5}{2}} e^{-\hat{\varepsilon}} d\hat{\varepsilon}.$$

Analytical solutions are only possible in certain cases:

2. $\nu_{\text{eff}} =$ constant (no energy dependence), and $l = 0$ for trapped particles

This is the case for trapped particles without energy-dependent collisions, with only the precession drift and no bounce frequency,

$$I_\varepsilon = \int_0^\infty \frac{\Omega_*^a + \Omega_n + \hat{\varepsilon}\Omega_*^b}{\hat{\varepsilon} + \Omega_n}\hat{\varepsilon}^{\frac{5}{2}} e^{-\hat{\varepsilon}} d\hat{\varepsilon}, \tag{39}$$

where $\Omega_n = (n\omega_E - \omega - i\nu_{\text{eff}})/(n\overline{\omega_D})$, $\Omega_*^a = (n\omega_{*N} - \frac{3}{2}n\omega_{*T} + i\nu_{\text{eff}})/(n\overline{\omega_D})$, $\Omega_*^b = \omega_{*T}/\overline{\omega_D}$, and $\omega_D = \overline{\omega_D}\hat{\varepsilon}$ (ie. $\overline{\omega_D}$ is the non-energy dependent portion of ω_D). The solution is given in Ref. [16], Eq. 30:

$$I_\varepsilon = \frac{15\sqrt{\pi}}{8}\Omega_*^b + 2\sqrt{\pi}\left(\Omega_n + \Omega_*^a - \Omega_n\Omega_*^b\right)\left[\frac{3}{8} - \frac{1}{4}\Omega_n + \frac{1}{2}\Omega_n^2 + i\frac{1}{2}\Omega_n^{\frac{5}{2}} Z\left(i\Omega_n^{\frac{1}{2}}\right)\right], \tag{40}$$

where Z is the plasma dispersion function.

MISK calculates the energy integral numerically, MARS-K does it analytically (cont.)

$$I_\varepsilon(\Psi,\Lambda,l)=\int_0^\infty \frac{n\left(\omega_{*N}+\left(\hat{\varepsilon}-\frac{3}{2}\right)\omega_{*T}\right)+n\omega_E-\omega_r-i\gamma}{n\left(\omega_D+(l+\alpha nq)\,\omega_b\right)-i\nu_{\rm eff}+n\omega_E-\omega_r-i\gamma}\hat{\varepsilon}^{\frac{5}{2}}e^{-\hat{\varepsilon}}d\hat{\varepsilon}.$$

Analytical solutions are only possible in certain cases:

3. $\nu_{\rm eff}=$ **constant (no energy dependence),** $l\neq 0$ **for trapped particles, and** $|\omega_D|\ll|l\omega_b|$

This is the case again without energy-dependent collisions, for trapped particles with $l\neq 0$ where the precession drift frequency is neglected with respect to the bounce frequency. If we now define $\Omega_{n2}=(n\omega_E-\omega-i\nu_{\rm eff})/(nl\overline{\omega_b})$, $\Omega_*^{a2}=(n\omega_{*N}-\frac{3}{2}n\omega_{*T}+i\nu_{\rm eff})/(nl\overline{\omega_b})$, $\Omega_*^{b2}=\omega_{*T}/l\overline{\omega_b}$, and $\omega_b=\overline{\omega_b}\hat{\varepsilon}^{\frac{1}{2}}$ (ie. $\overline{\omega_b}$ is the non-energy dependent portion of ω_b), then

$$I_\varepsilon=\int_0^\infty\frac{\Omega_*^{a2}+\Omega_{n2}+\hat{\varepsilon}\Omega_*^{b2}}{\frac{\overline{\omega_D}}{l\overline{\omega_b}}\hat{\varepsilon}+\hat{\varepsilon}^{\frac{1}{2}}+\Omega_{n2}}\hat{\varepsilon}^{\frac{5}{2}}e^{-\hat{\varepsilon}}d\hat{\varepsilon}. \tag{43}$$

With $\overline{\omega_D}/l\overline{\omega_b}\to 0$ this has the analytical solution

$$\begin{aligned}I_\varepsilon=&-\Omega_*^{b2}\left(\frac{15\sqrt{\pi}}{8}\Omega_{n2}-6\right)+2\sqrt{\pi}\left(\Omega_{n2}+\Omega_*^{a2}+\Omega_{n2}^2\Omega_*^{b2}\right)\left[-\Omega_{n2}\left(\frac{3}{8}+\frac{1}{4}\Omega_{n2}^2+\frac{1}{2}\Omega_{n2}^4\right)-\frac{1}{2}\Omega_{n2}^6Z\left(\Omega_{n2}\right)\right.\\&\left.+\frac{1}{2\sqrt{\pi}}\left(\Omega_{n2}^4+\Omega_{n2}^2+2\right)+\frac{1}{2\sqrt{\pi}}e^{-\Omega_{n2}^2}\left(i\pi-\mathrm{Ei}(\Omega_{n2}^2)+\frac{1}{2}\ln(\Omega_{n2}^2)-\frac{1}{2}\ln(\Omega_{n2}^{-2})-2\ln(\Omega_{n2})\right)\right].\end{aligned} \tag{44}$$

MISK used to compare numerical/ analytical solution of I_e for ITER case: compares well*

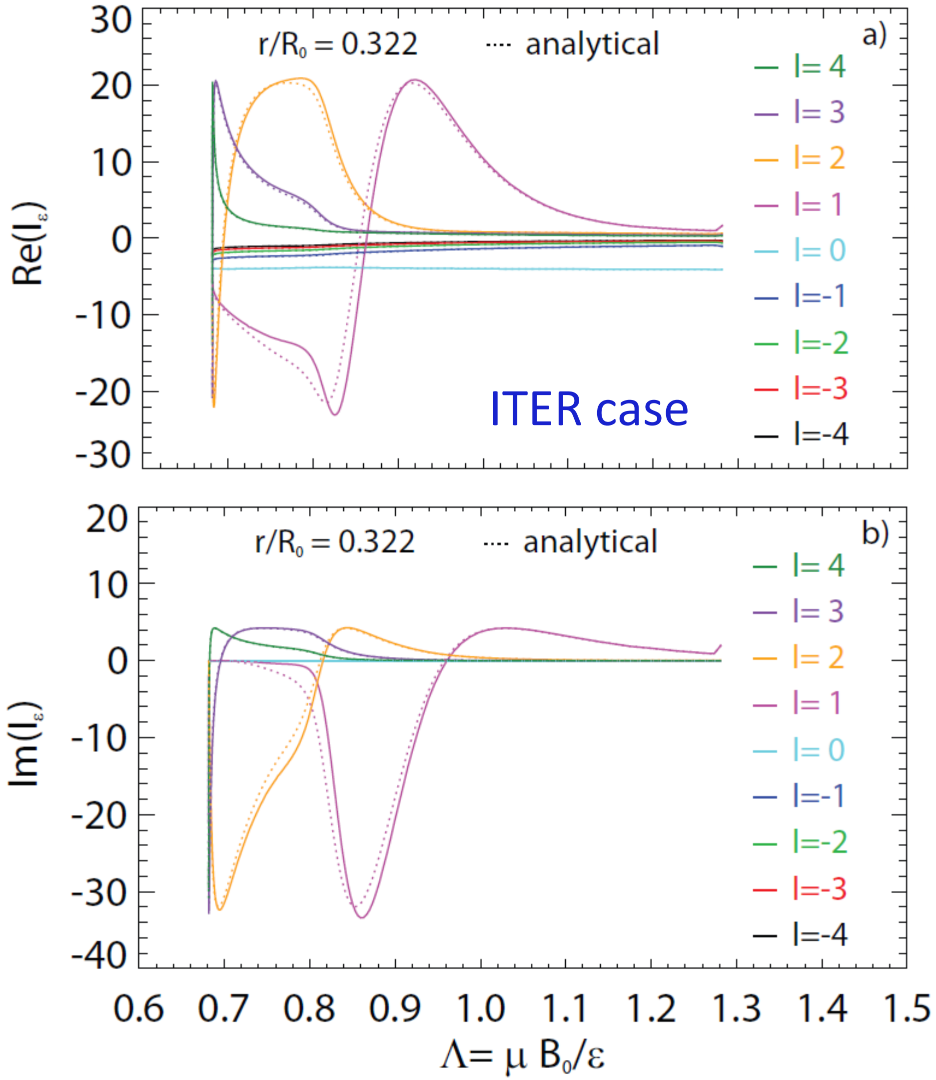

- Reasonable agreement gives confidence that MISK is properly computing the energy integral
  - Useful when comparing to other codes
  - Similar calculation made for both Solov'ev 1 and 3 cases using MISK
    - Also found that numerical computation compares well to analytical
  - *Note: calculation for trapped thermal ions

Convergence study vs. damping parameter shows no issues with zero damping

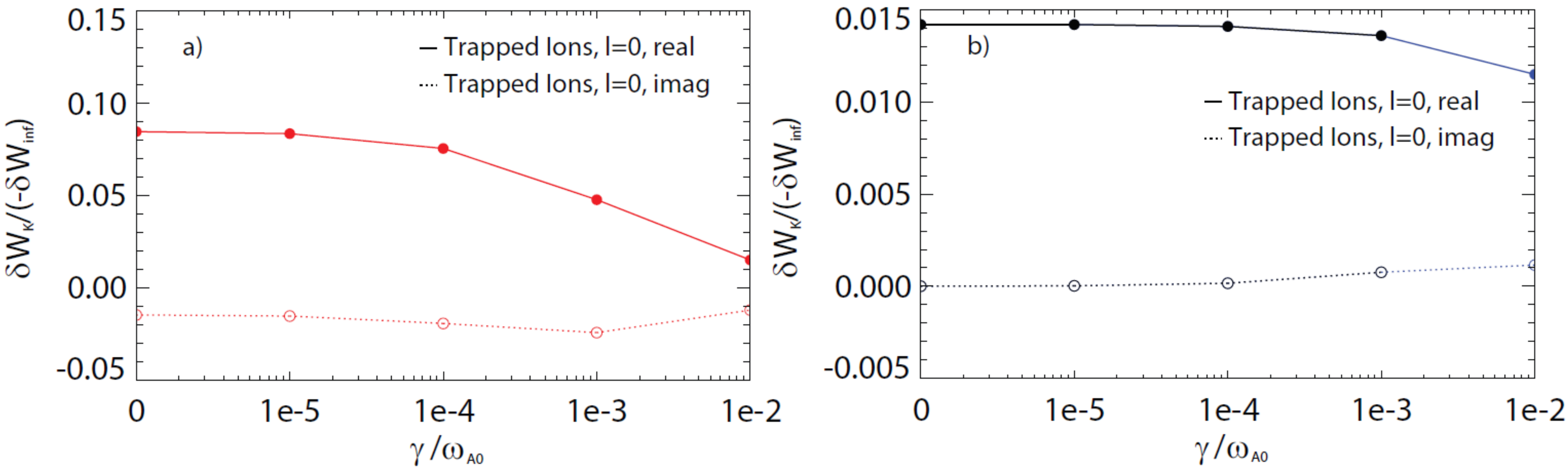

FIG. 24. Convergence of δW_K versus damping for the Solov'ev 1 case, as calculated by a) MARS-K, and b) MISK. For MISK, blue indicates numerical evaluation of the energy integral and black indicates analytical.

- Damping from either collisions or mode growth rate.
- Both codes converge, but to different values.

Kruskal-Oberman limit calculations performed: MISK and MARS-K results differ by 50% (should be closer)

In the Kruskal-Oberman limit , $|\omega_E - \omega| \to \infty$ and therefore

$$I_\varepsilon(\Psi, \Lambda, l) \to I_\varepsilon^{KO} = \int_0^\infty \hat{\varepsilon}^{\frac{5}{2}} e^{-\hat{\varepsilon}} d\hat{\varepsilon} = \frac{15\sqrt{\pi}}{8}.$$

In this limit δW_K is purely real, and independent of the mode-particle resonances. This allows a good check on the $|\langle H/\hat{\varepsilon}\rangle|^2$ part of the problem.

$\delta W_K/-\delta W_\infty$ for MISK (blue) and MARS-K (red)

	thermal ions			thermal electrons			Total
	trapped		circulating	trapped		circulating	
	$l=0$	$l\neq 0$		$l=0$	$l\neq 0$		
Solov'ev 1	1.11×10^{-2}	1.02×10^{-2}	9.69×10^{-2}	1.11×10^{-2}	1.02×10^{-2}	9.69×10^{-2}	1.57×10^{-1} 2.36×10^{-1}
Solov'ev 3	1.16×10^{-1}	4.84×10^{-2}	1.80×10^{-1}	1.16×10^{-1}	4.84×10^{-2}	1.80×10^{-1}	6.89×10^{-1}
ITER	5.83×10^{-1}	5.20×10^{-1}	2.74	7.02×10^{-1}	6.01×10^{-1}	3.30	8.46

- Major simplification (I_ε = constant) gives key clue to issue
  - Different indicates the issue is in the perturbed Lagrangian.
  - Solution to differences in Lagrangian may eliminate most of the problem.

MARS-K and MISK energy integrals now agree* for Solov'ev 1 equilibrium

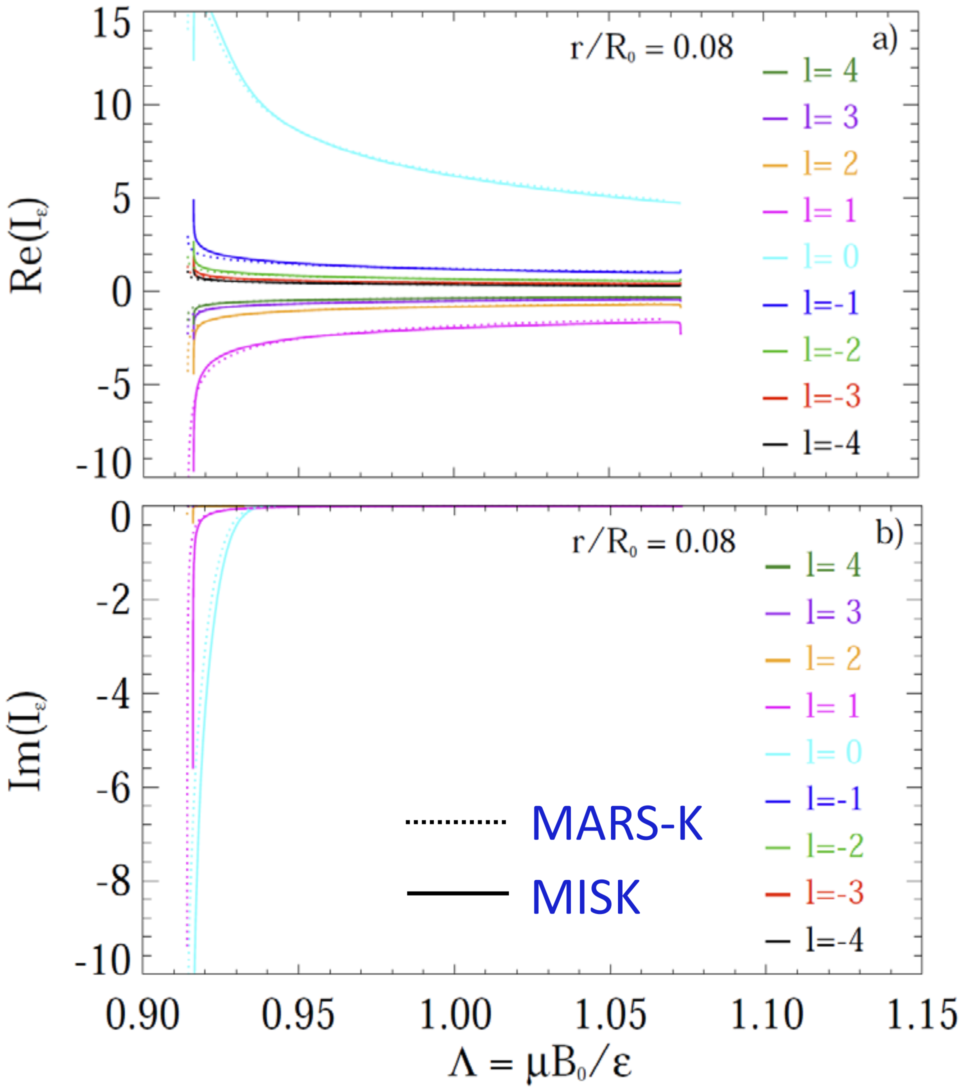

- Attaining agreement
  - Required properly matching frequency inputs
  - Flip sign of imaginary part
  - Positive l in MISK is negative in MARS-K
    - Because of MARS-K left-handed coordinate system?
  - *Note: calculation for trapped thermal ions
    - Expand to all particles

XXX

MARS-K adopts an MHD – drift kinetic hybrid formulation for both thermal & hot particles

$$(\gamma + in\Omega)\xi = \mathbf{v} + (\xi \cdot \nabla\Omega)R^2\nabla\phi,$$

$$\rho(\gamma + in\Omega)\mathbf{v} = -\nabla \cdot \mathbf{p} + \mathbf{j} \times \mathbf{B} + \mathbf{J} \times \mathbf{Q} - \rho\left[2\Omega\hat{\mathbf{Z}} \times \mathbf{v} + (\mathbf{v} \cdot \nabla\Omega)R^2\nabla\phi\right],$$

$$(\gamma + in\Omega)\mathbf{Q} = \nabla \times (\mathbf{v} \times \mathbf{B}) + (\mathbf{Q} \cdot \nabla\Omega)R^2\nabla\phi,$$

$$(\gamma + in\Omega)p = -\mathbf{v} \cdot \nabla P,$$

$$\mathbf{j} = \nabla \times \mathbf{Q},$$

$$\mathbf{p} = p\mathbf{I} + p_{\parallel}\hat{\mathbf{b}}\hat{\mathbf{b}} + p_{\perp}(\mathbf{I} - \hat{\mathbf{b}}\hat{\mathbf{b}}),$$

Self-consistent MHD-kinetic coupling

$$p_{\parallel}e^{-i\omega t + in\phi} = \sum_{e,i}\int d\Gamma M v_{\parallel}^2 f_{th}^1(\xi_\perp) + \int d\Gamma M v_{\parallel}^2 f_h^1(\xi_\perp)$$

$$p_{\perp}e^{-i\omega t + in\phi} = \sum_{e,i}\int d\Gamma \frac{1}{2} M v_{\perp}^2 f_{th}^1(\xi_\perp) + \int d\Gamma \frac{1}{2} M v_{\perp}^2 f_h^1(\xi_\perp)$$

thermal

Energetic particles

Y. Liu

CCFE CULHAM CENTRE FOR FUSION ENERGY

Research Councils UK Energy For a Low Carbon Future

HAGIS Suite of codes (+references) - Stability

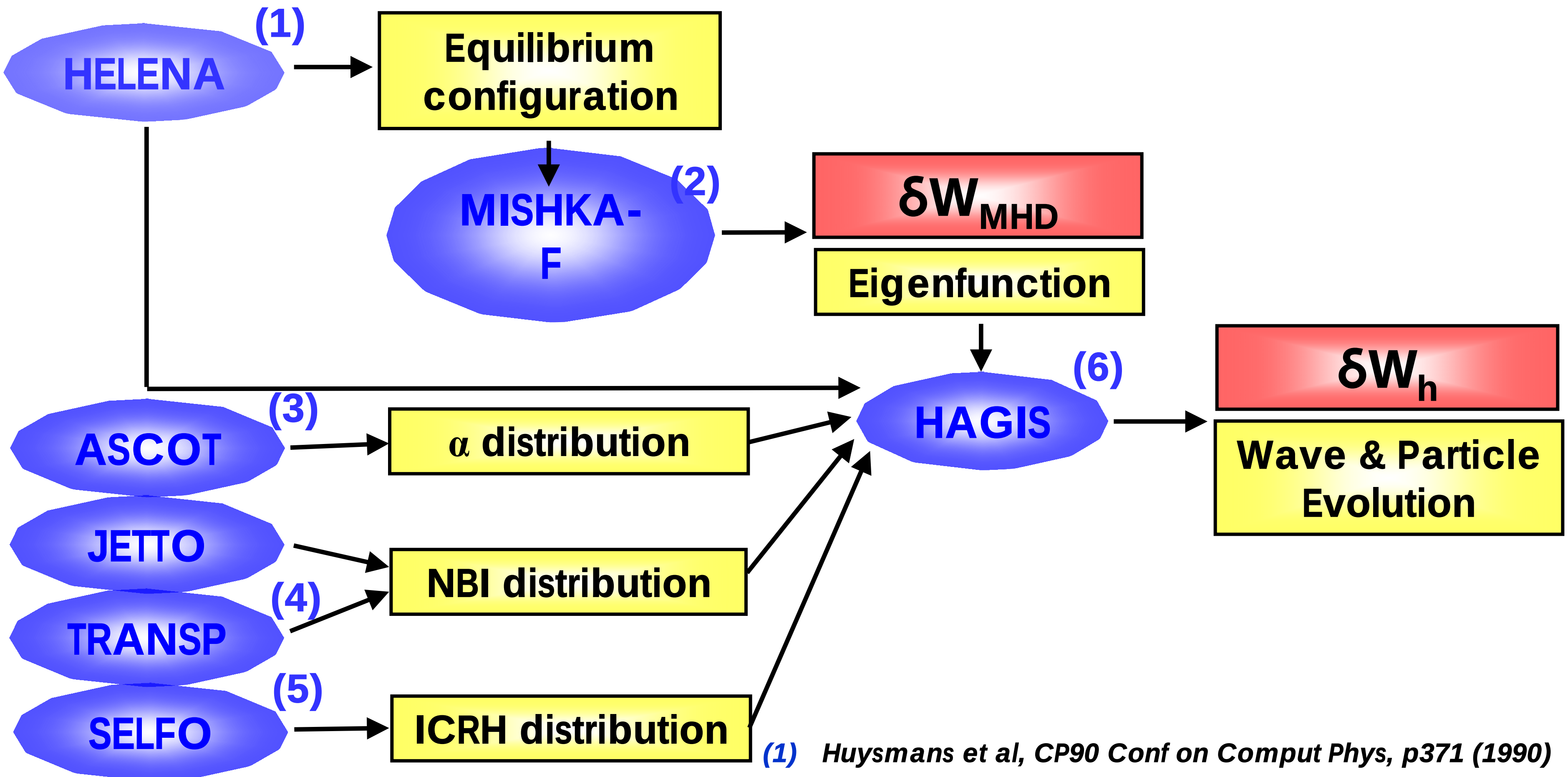

(1) Huysmans et al, CP90 Conf on Comput Phys, p371 (1990)

(2) Chapman et al, Phys Plasmas, 13, 062511 (2006)

(3) JA Heikennen et al, Comput. Phys. Comm., 76, 215 (1993)

(4) Budny et al, Nucl Fusion, 32, 429 (1992)

(5) Hedin et al, Nucl Fusion, 42, 527 (2002)

(6) Pinches et al, Comput Phys Commun, 111, 133 (1998)

I. Chapman

CCFE CULHAM CENTRE FOR FUSION ENERGY

Research Councils UK Energy For a Low Carbon Future

Started code comparison with simple equilibria and profile assumptions

Solov'ev case 1 (near-circular) Solov'ev case 3 (shaped)

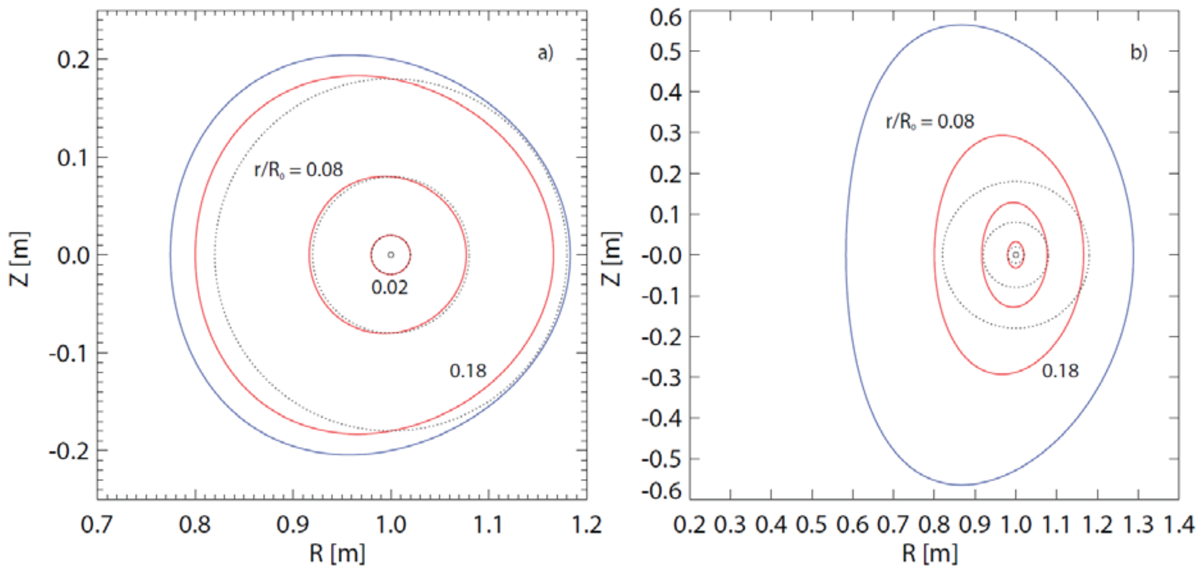

$$\mu_0 P(\psi) = -\frac{1+\kappa^2}{\kappa R_0^3 q_0}\psi, \quad F(\psi) = 1$$

$$\psi = \frac{\kappa}{2R_0^3 q_0}\left[\frac{R^2 Z^2}{\kappa^2} + \frac{1}{4}\left(R^2 - R_0^2\right)^2 - a^2 R_0^2\right]$$

$$\delta W_K \propto \int \left[\frac{\omega_{*N} + \left(\hat{\varepsilon} - \frac{3}{2}\right)\omega_{*T} + \omega_E}{\langle\omega_D\rangle + l\omega_b + \omega_E}\right]\hat{\varepsilon}^{\frac{5}{2}} e^{-\hat{\varepsilon}} d\hat{\varepsilon}$$

Simplified resonant denominator due to assumptions

- Common ground for codes (MARS / HAGIS / MISK)
  - Solov'ev equilibria
  - Codes run in perturbative mode
  - Density gradient constant
  - No energetic particles
  - ω_r, γ, $\nu_{eff} = 0$

Expanded comparison to include ITER equilibrium

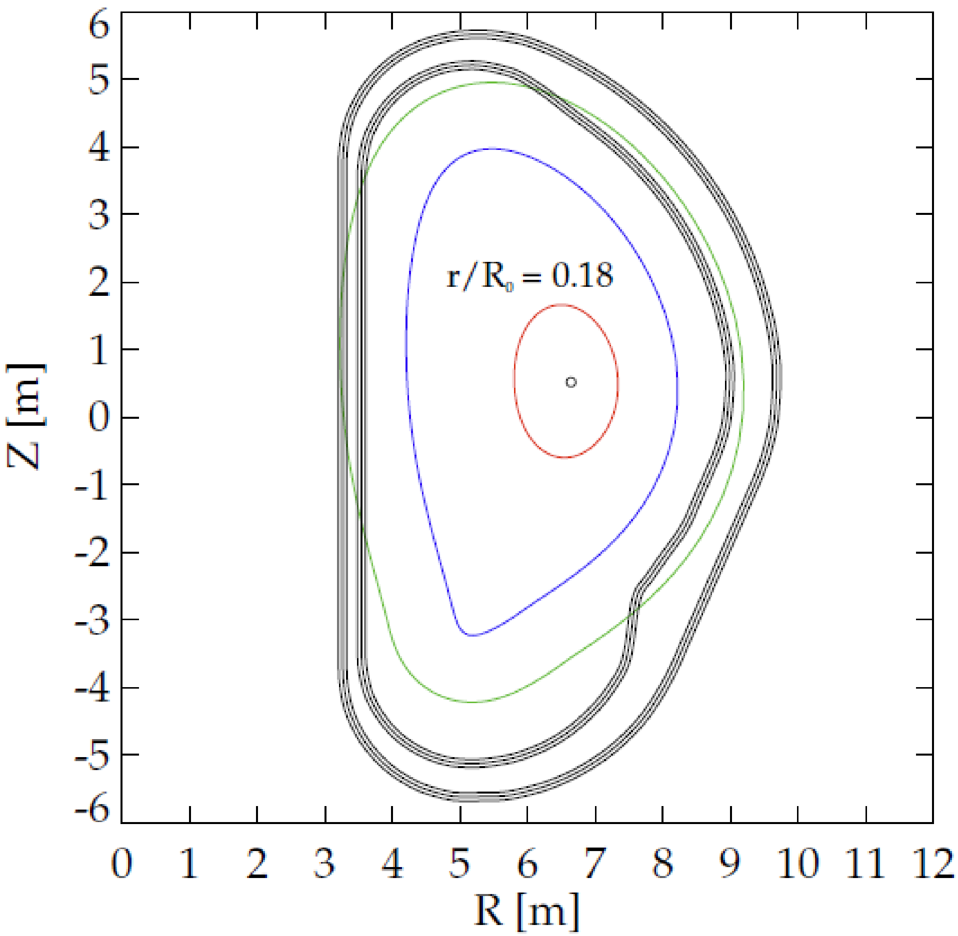

- More realistic case (ITER)
  - ITPA MHD WG7 equilibrium
    - I_p = 9 MA, β_N = 2.9 (7% above n = 1 no-wall limit)
  - Codes run in perturbative mode
  - With/without energetic particles
  - ω_r, γ, ν_{eff} = 0

$$\delta W_K \propto \int \left[\frac{\omega_{*N} + \left(\hat{\varepsilon} - \frac{3}{2}\right)\omega_{*T} + \omega_E}{\langle \omega_D \rangle + l\omega_b + \omega_E} \right] \hat{\varepsilon}^{\frac{5}{2}} e^{-\hat{\varepsilon}} d\hat{\varepsilon}$$

Note: Simplified resonant denominator due to assumptions

Shaped vs. near-circular Solov'ev cases have important q profile differences for benchmarking

Solov'ev case 1 (near-circular)

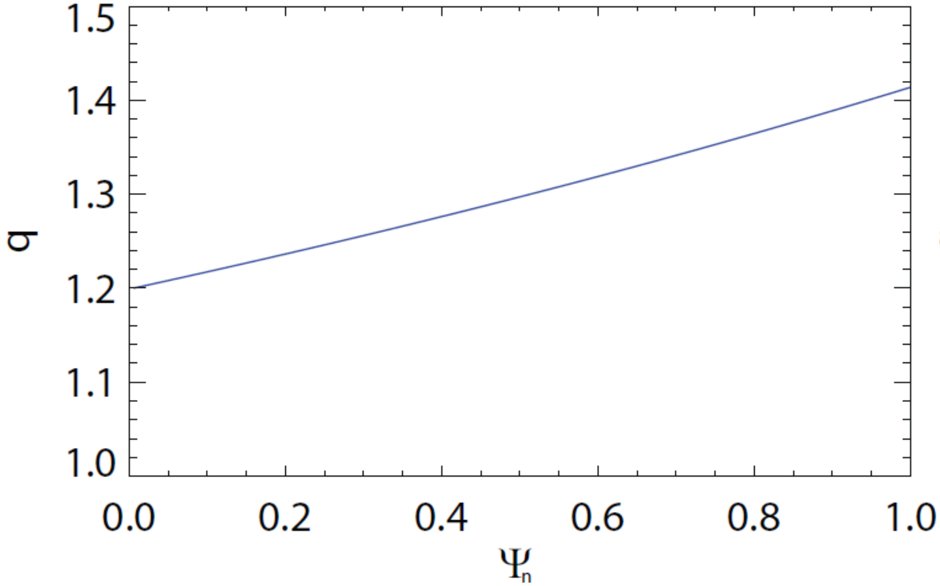

Solov'ev case 3 (shaped)

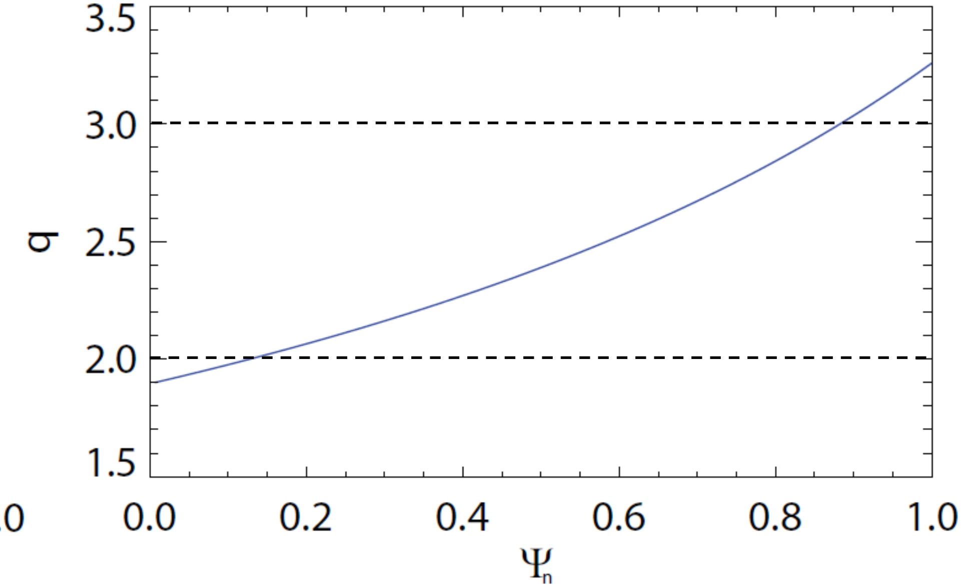

- No n = 1 rational surfaces
  - Eliminates potential differences between calculation of kinetic dissipation at rational surfaces
- Simple, key n = 1 rational surfaces
  - q = 2, 3 surfaces in the plasma
- ITER equilibrium: rev. shear, $q_0 \sim 2.2$, $q_{min} \sim 1.7$, $q_a \sim 7.1$

Differences in how MARS, MISK, HAGIS consider mode dissipation at rational surfaces is thought to be key – will be a main focus of next steps

The kinetic term can be split into two pieces that depend on the eigenfunction or the frequencies, for code comparison

$$\delta W_K = -\frac{\sqrt{\pi}}{2}\int_0^{\Psi_a}\frac{nT}{B_0}\int_{B_0/B_{\max}}^{B_0/B_{\min}}\tau\sum_l |\langle H/\hat{\varepsilon}\rangle|^2 I_{\hat{\varepsilon}}\, d\Lambda d\Psi.$$

Solov'ev case 1 (near-circular)

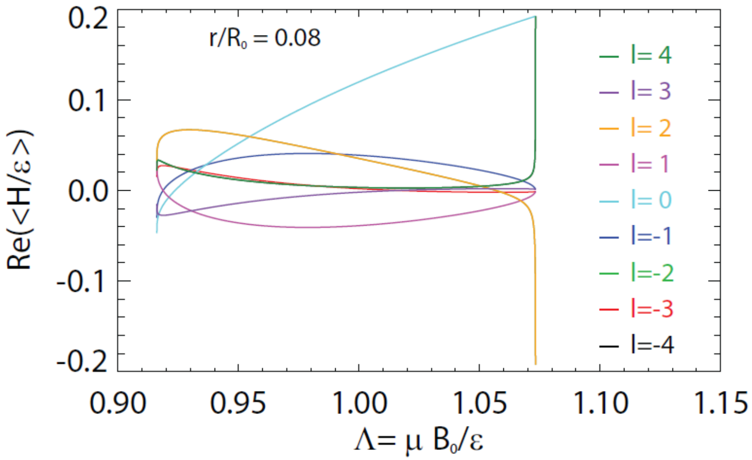

Perturbed Lagrangian

$$\langle H/\hat{\varepsilon}\rangle(\Psi,\Lambda,l) = \frac{1}{\tau}\oint\frac{1}{\sqrt{1-\frac{\Lambda B}{B_0}}}\left[\left(2-3\frac{\Lambda B}{B_0}\right)(\boldsymbol{\kappa}\cdot\boldsymbol{\xi}_\perp) - \left(\frac{\Lambda B}{B_0}\right)(\nabla\cdot\boldsymbol{\xi}_\perp)\right]e^{-il\omega_b t}d\ell.$$

- Depends mostly on the eigenfunction.

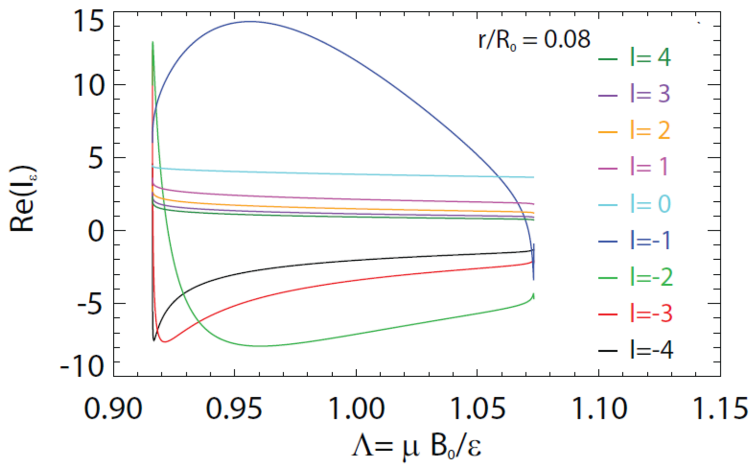

Energy integral of the frequency resonance fraction

$$I_\varepsilon(\Psi,\Lambda,l) = \int_0^\infty \frac{\omega_{*N} + \left(\hat{\varepsilon}-\frac{3}{2}\right)\omega_{*T} + \omega_E - \omega_r - i\gamma}{\omega_D + l\omega_b + \omega_E - i\nu_{\text{eff}} - \omega_r - i\gamma}\hat{\varepsilon}^{\frac{5}{2}}e^{-\hat{\varepsilon}}d\hat{\varepsilon}.$$

- Does not depend on eigenfunction, just frequency profiles

Eigenfunction benchmarking calculations were made to yield similar eigenfunctions, which are verified

Solov'ev case 1 (near-circular) | Solov'ev case 3 (shaped) | ITER

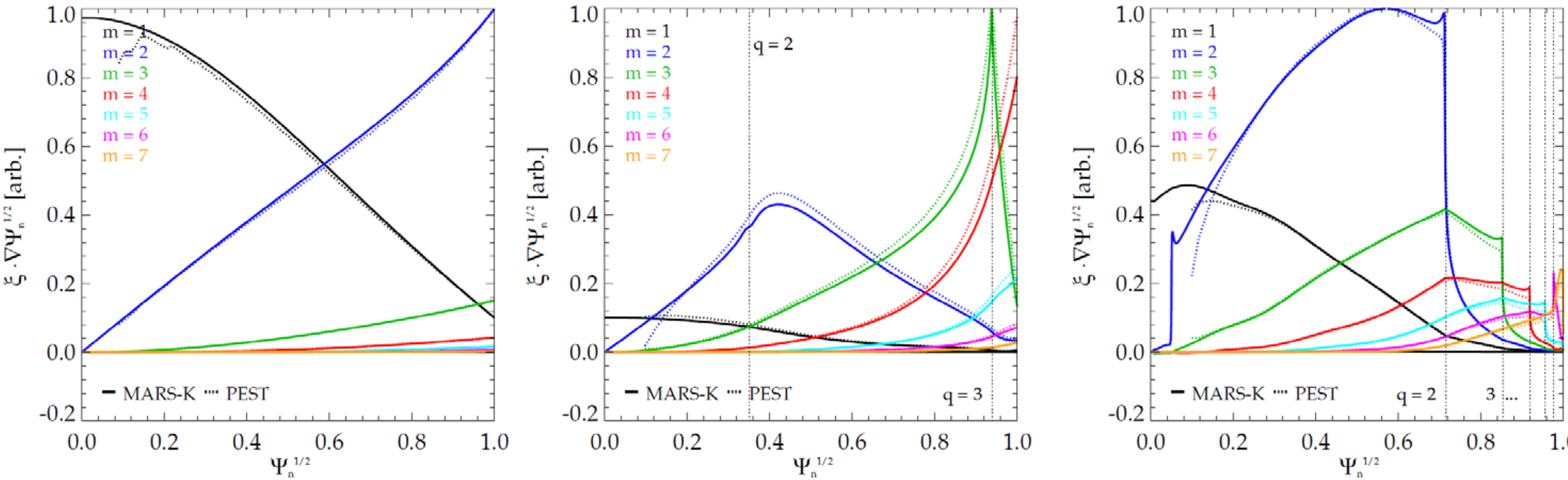

- PEST, MARS-K compared with-wall RWM
  - In PEST we use the wall position that yields marginal stability
  - PEST, MARS-K, and MISHKA compared for no-wall ideal kink
- There are some differences at rational surfaces
  - May lead to stability differences between MISK and MARS-K calculations

Bounce frequency vs. pitch angle compares well between codes

Solov'ev case 1 (near-circular)

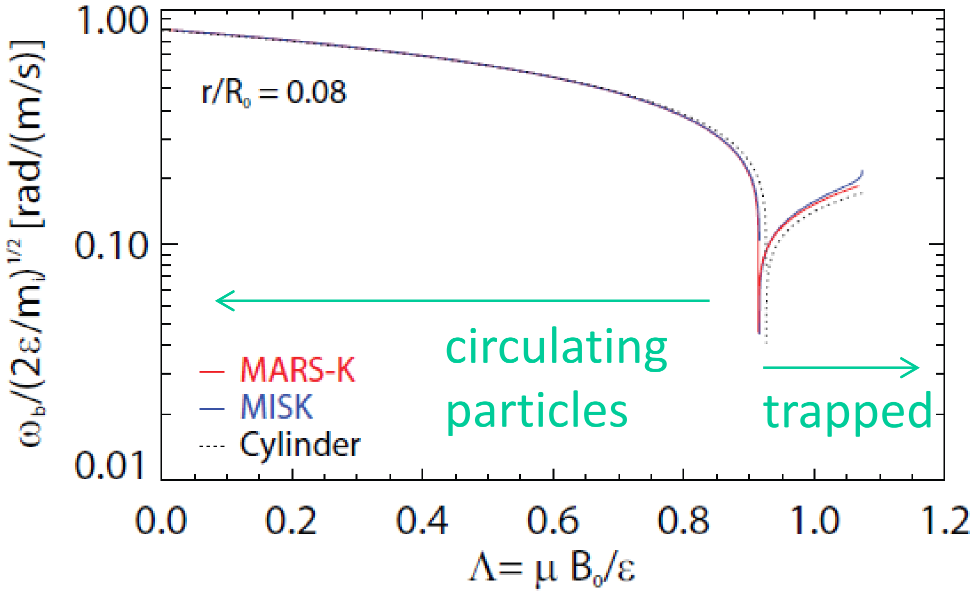

Solov'ev case 3 (shaped)

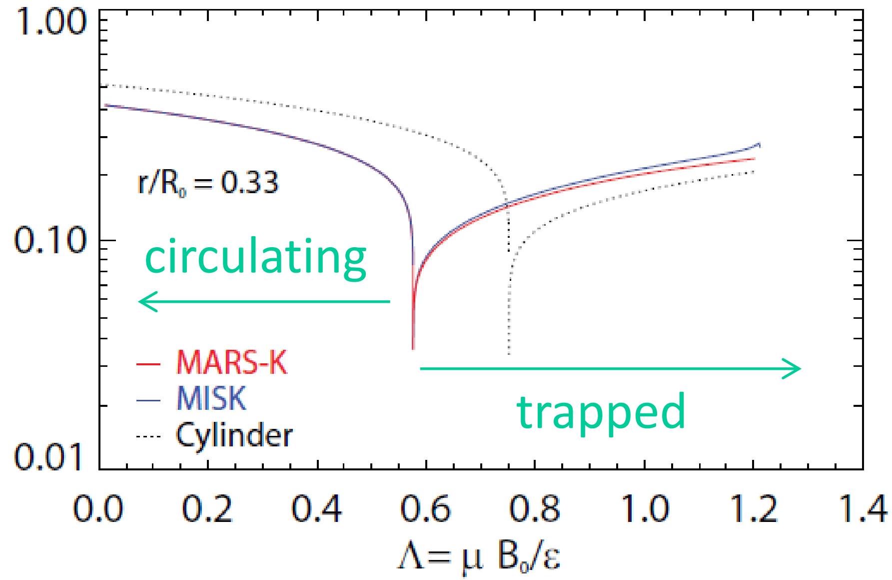

$$\frac{\omega_b}{\sqrt{2\varepsilon/m_i}} = \frac{\sqrt{2\epsilon_r \Lambda B_0}}{4qR_0}\frac{\pi}{K(k)} \quad \text{(trapped)}$$

$$k = \left[\frac{1-\Lambda B_0 + \epsilon_r \Lambda B_0}{2\epsilon_r \Lambda B_0}\right]^{\frac{1}{2}}$$

$$\frac{\omega_b}{\sqrt{2\varepsilon/m_i}} = \frac{\sqrt{1-\Lambda B_0 + \epsilon_r \Lambda B_0}}{2qR_0}\frac{\pi}{K(1/k)} \quad \text{(circulating)}$$

<u>large aspect ratio approximation</u>

here, ϵ_r is the inverse aspect ratio, s is the magnetic shear, K and E are the complete elliptic integrals of the first and second kind, and $\Lambda = \mu B_0/\varepsilon$, where μ is the magnetic moment and ε is the kinetic energy.

Bounce and precession drift frequency radial profiles agree (deeply trapped regime shown)

Bounce frequency

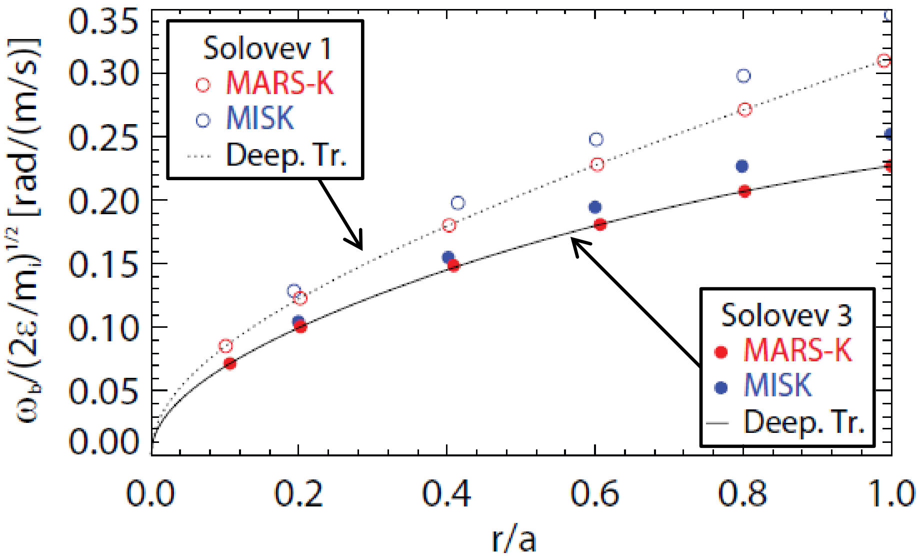

Precession drift frequency

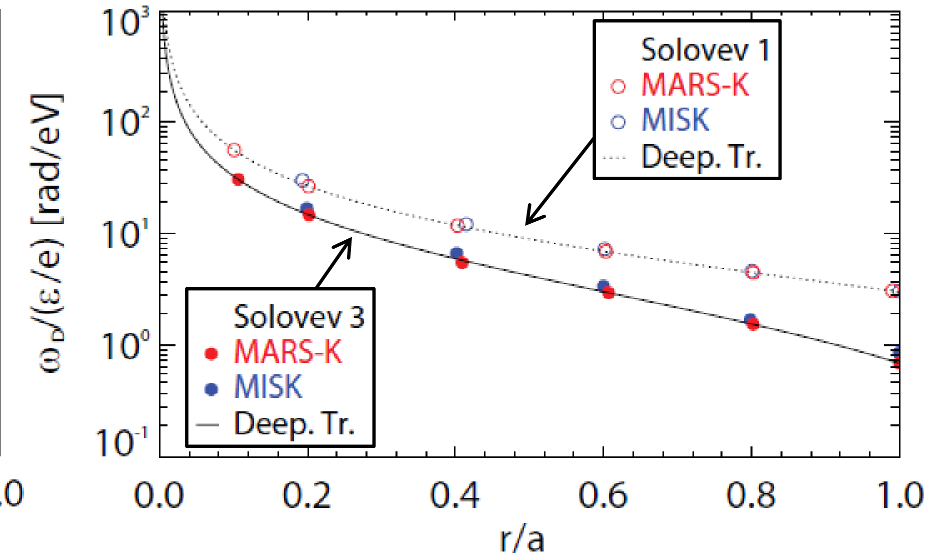

<u>Deeply trapped limit</u>

$$\frac{\omega_b}{\sqrt{2\varepsilon/m_i}} = \frac{1}{q_0}\left(\frac{F^2}{1+2\epsilon_r}+\frac{\kappa^2\epsilon_r^2}{q_0^2}\right)^{-1}\left[\frac{F^2\epsilon_r}{2\left(1+2\epsilon_r\right)}+\frac{\kappa^2\epsilon_r^3}{q_0^2}+\frac{\left(1-\kappa^2\right)\epsilon_r^2}{2q_0^2}\left(1+2\epsilon_r\right)\right]^{\frac{1}{2}}$$

- Good agreement across entire radial profile

<u>Significant issue found:</u> precession drift frequencies did not agree

Solov'ev case 1 (near-circular)

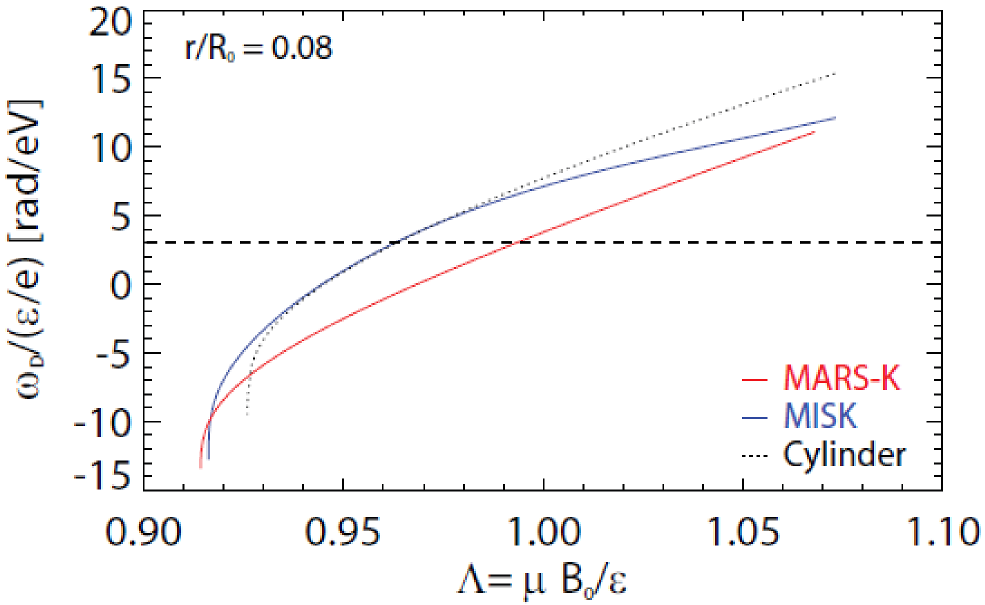

Solov'ev case 3 (shaped)

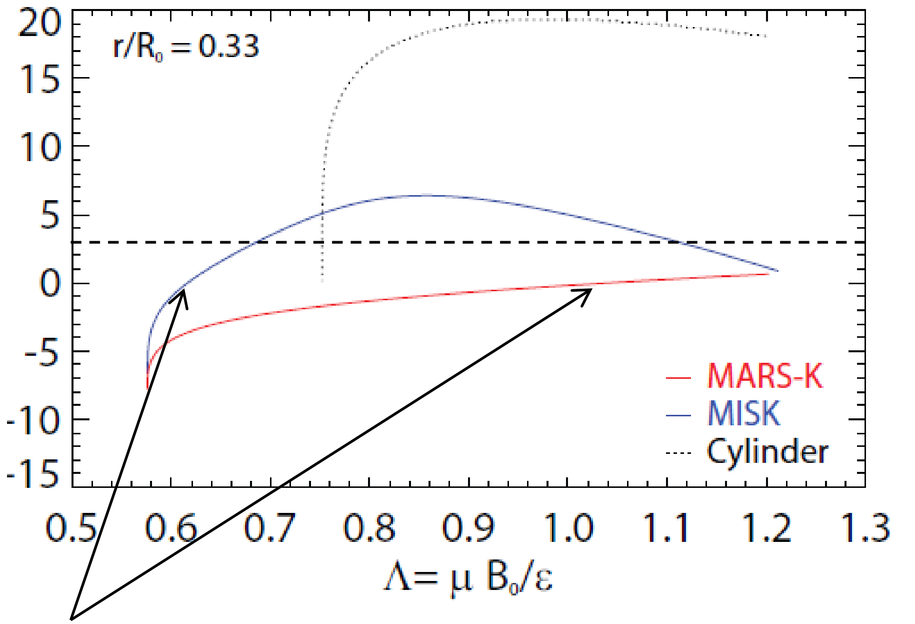

- Clear difference in drift reversal point, even in near-circular case
- <u>Issue found and corrected</u>: metric coefficients for non-orthogonal grid incorrect in PEST interface to MISK

<u>large aspect ratio approximation</u>

$$\frac{\langle \omega_D \rangle}{\varepsilon / e} = \frac{2q\Lambda}{R_0^2 B_0 \epsilon_r}\left[(2s+1)\frac{E\left(k^2\right)}{K\left(k^2\right)} + 2s\left(k^2 - 1\right) - \frac{1}{2}\right] \qquad k = \left[\frac{1 - \Lambda + \epsilon_r \Lambda}{2\epsilon_r \Lambda}\right]^{\frac{1}{2}}$$

[Jucker et al., Phys. Plasmas 15, 112503 (2008)]

Significant issue resolved:
The precession drift frequencies now agree

Solov'ev case 1 (near-circular)

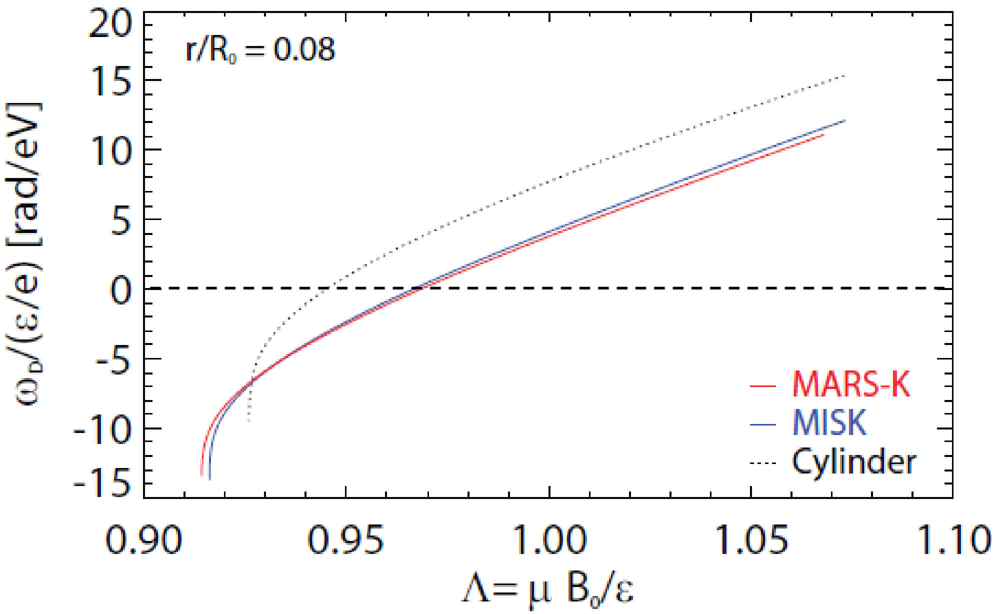

Solov'ev case 3 (shaped)

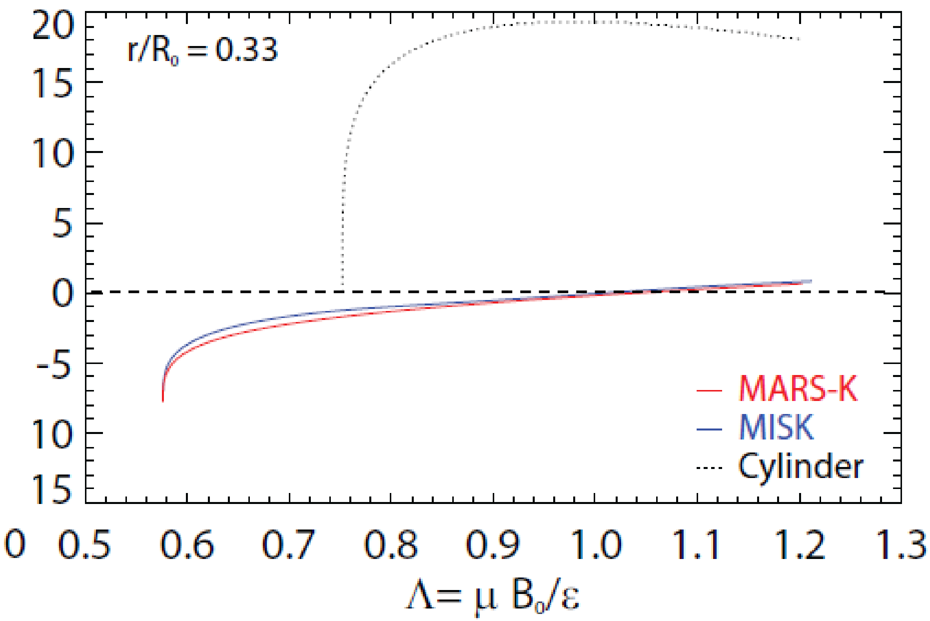

- Metric coefficients corrected in PEST interface to MISK

$$\omega_D = -\frac{1}{\tau}\int \frac{1}{v_\parallel}\mathbf{v_D}\cdot(\boldsymbol{\nabla}\phi - \hat{q}\boldsymbol{\nabla}\theta)\,d\ell - \frac{1}{\tau}\int_{\theta(t)}^{\theta(t')}\hat{q}\,d\theta.$$

if Ψ and θ are orthogonal:

$$\hat{q}\mathbf{B}\times\boldsymbol{\nabla}\theta = \frac{(\mathbf{B}_\phi\cdot\boldsymbol{\nabla}\phi)\,(\mathbf{B}_\phi\times\boldsymbol{\nabla}\theta)}{\mathbf{B}_\theta\cdot\boldsymbol{\nabla}\theta}$$

But in PEST, Ψ and θ are non-orthogonal:

$$\hat{q}\mathbf{B}\times\boldsymbol{\nabla}\theta = \frac{\mathbf{B}_\phi\cdot\boldsymbol{\nabla}\phi}{(\mathbf{B}_\phi\cdot\boldsymbol{\nabla}\theta + \mathbf{B}_\theta\cdot\boldsymbol{\nabla}\theta)}\,(\mathbf{B}_\phi\times\boldsymbol{\nabla}\theta + \mathbf{B}_\theta\times\boldsymbol{\nabla}\theta)$$

How does ω_D correction effect NSTX results? Mostly affects outer surfaces; characteristic change of $\gamma\tau_w$ with ω_ϕ is the same.

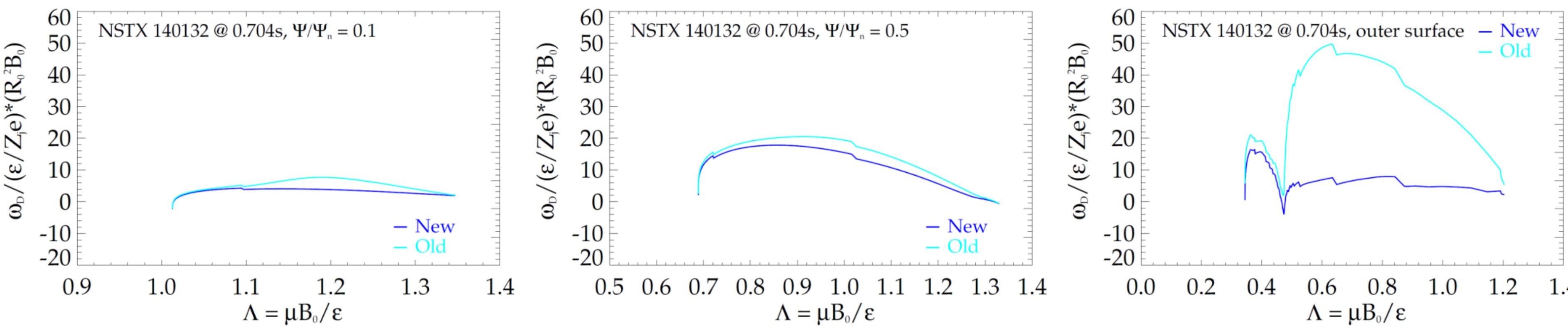

RWM stability vs. ω_ϕ (contours of $\gamma\tau_w$)

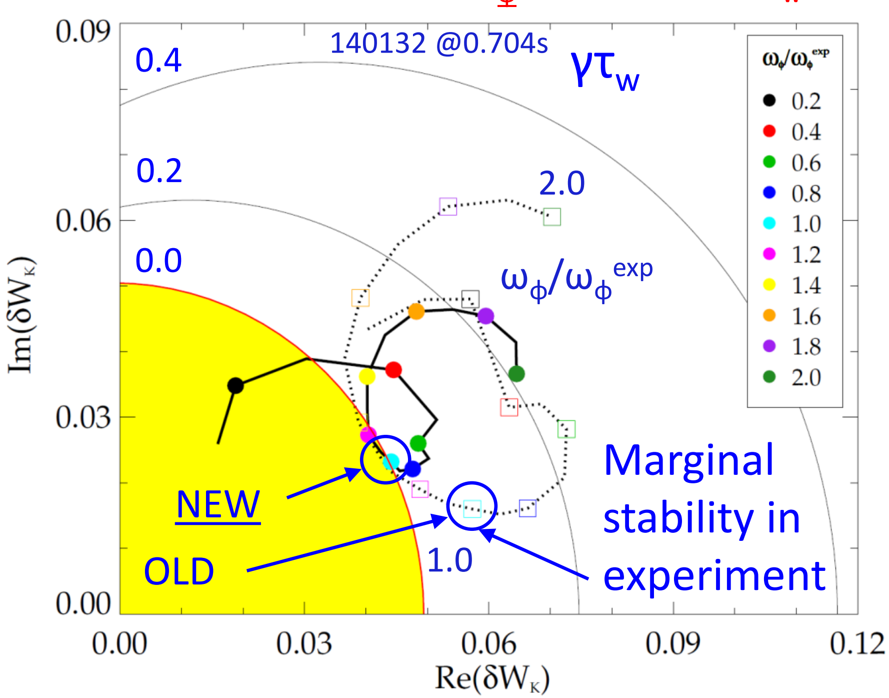

- Affects magnitude of δW_K, but not trends
- In this case, agreement with the experimental marginal point improves
  - Calculations continue to determine the effect of the correction on wider range of cases